Mechano-electrical interactions and heterogeneities in wild-type and drug-induced long QT syndrome rabbits

R.D. Lewetag*[1,2], S. Nimani*[3], N. Alerni*[3], T. Hornyik*[1,2,3], S.F. Jacobi [2,4], R. Moss [2,5], M. Menza [6], N. Pilia [7], T. Puig Walz[2,5], A. HajiRassouliha[8], S. Perez-Feliz [2], M. Zehender [1], G. Seemann [2], C.M. Zgierski-Johnston [2], R. Lopez [3], K.E. Odening [1,3]

1 Department of Cardiology and Angiology I, University Heart Center Freiburg, University Medical Center Freiburg, Freiburg, Germany

2 Institute for Experimental Cardiovascular Medicine, University Heart Center Freiburg – Bad Krozingen and Faculty of Medicine, University of Freiburg, Freiburg, Germany

3 Translational Cardiology, Department of Cardiology and Department of Physiology, University Hospital Bern, Bern, Switzerland

4 Department of Congenital Heart Defects and Pediatric Cardiology, University Heart Center Freiburg, Faculty of Medicine, University of Freiburg, Freiburg, Germany

5 Fraunhofer Institute for High-Speed Dynamics, Ernst-Mach-Institute EMI, Freiburg, Germany

6 Department of Radiology, Medical Physics, University Hospital Freiburg, and Faculty of Medicine, University of Freiburg, Germany

7 Karlsruhe Institute of Technology, Karlsruhe, Germany

8 Auckland Bioengineering Institute, Auckland, New Zealand

This is an Accepted Article that has been peer-reviewed and approved for publication in The Journal of Physiology, but has yet to undergo copy-editing and proof correction. Please cite this article as an 'Accepted Article'; doi: 10.1113/jphysiol.2023.15560.

Corresponding Author

Prof. Dr. med Katja E. Odening, MD

Professor of Translational Cardiology

Department of Physiology and Department of Cardiology

University Bern and University Hospital Bern

Buehlplatz 5

CH-3012 Bern

Switzerland

katja.odening@unibe.ch / katja.odening@insel.ch

Key point summary

- Electromechanical reciprocity – comprising excitation-contraction coupling (EMC) and mechano-electric feedback loops (MEC) – is essential for physiological cardiac function.
- Alterations in electrical and/or mechanical heterogeneity are known to have potentially pro-arrhythmic effects.
- In this study, we aimed to investigate how electrical changes impact on the mechanical function (EMC) and vice versa (MEC) – both under physiological conditions (control) and in acquired long QT syndrome (aLQTS).
- We show that changing the electrical function (in aLQTS) results in significantly altered mechanical heterogeneity via EMC and – vice versa – that increasing the preload acutely prolongs repolarization duration and increases electrical heterogeneity, particularly in aLQTS as compared to control.
- Our results substantiate the hypothesis that LQTS is an 'electro-mechanical' – rather than a 'purely electrical' – disease and suggest that acute MEC effects may play an additional role in LQT-related arrhythmogenesis.

Abstract

Background: Electromechanical reciprocity – comprising electro-mechanical (EMC) and mechano-electric coupling (MEC) – provides cardiac adaptation to changing physiological demands. Understanding electromechanical reciprocity and its impact on function and heterogeneity in pathological conditions – such as (drug-induced) acquired long QT syndrome (aLQTS) – might lead to novel insights in arrhythmogenesis. Our aim is to investigate how electrical changes impact on mechanical function (EMC) and vice versa (MEC) under physiological conditions and in aLQTS.

Methods: To measure regional differences in EMC and MEC *in vivo*, we used tissue phase mapping cardiac MRI and 24-lead ECG vest in healthy (control) and I_{Kr}-blocker E-4031-induced aLQTS rabbit

hearts. MEC was studied *in vivo* by acutely increasing cardiac preload, and *ex vivo* by using voltage optical mapping in beating hearts at different preloads.

Results: In aLQTS, electrical repolarization (heart rate corrected RT-interval, RTn370) was prolonged compared to control ($p<0.0001$) with increased spatial and temporal RT heterogeneity ($p<0.01$). Changing electrical function (in aLQTS) resulted in significantly reduced diastolic mechanical function and prolonged contraction duration (EMC), causing increased apico-basal mechanical heterogeneity. Increased preload acutely prolonged RTn370 in both control and aLQTS hearts (MEC). This effect was more pronounced in aLQTS ($p<0.0001$). Additionally, regional RT-dispersion increased in aLQTS. Motion-correction allowed to determine APD-prolongation in beating aLQTS hearts, but limited motion correction accuracy upon preload-changes prevented a clear analysis of MEC *ex vivo*.

Conclusion: Mechano-induced RT-prolongation and increased heterogeneity were more pronounced in aLQTS than in healthy hearts. Acute MEC effects may play an additional role in LQT-related arrhythmogenesis, warranting further mechanistic investigations.

Introduction

Electrical and mechanical heterogeneity are an important prerequisite for physiological cardiac function (Janse *et al.*, 2012; Solovyova *et al.*, 2016). Driven by regional heterogeneities in the expression of cardiac ion channels, electro-mechanical heterogeneity exists between right and left ventricles (RV, LV), in apico-basal and transmural directions (Antzelevitch & Fish, 2001; Janse *et al.*, 2012; Solovyova *et al.*, 2016). Acute or chronic changes in electrical function can alter mechanical function and vice versa – via electro-mechanical (EMC) and mechano-electric (MEC) coupling (Quinn & Kohl, 2021). Recently denominated as "electromechanical reciprocity" (Odening *et al.*, 2022), it is responsible for alterations in both global and local electro-mechanical function (leading to heterogeneity). A variety of different stretch-activated or stretch-sensitive channels have been identified as mediators of MEC (Quinn & Kohl, 2021).

Electromechanical reciprocity is not only present in healthy hearts, but can also be observed and accentuated in "electrical" heart diseases such as long QT syndrome (LQTS), in which cardiac repolarization and the QT interval are prolonged and patients are prone to ventricular tachycardia, arrhythmic syncope, and sudden cardiac death (Roden, 2008). LQTS can either be inherited due to mutations in genes encoding for cardiac ion channels (Schwartz *et al.*, 2012) or – more frequently – acquired (Roden, 2004) as a result of drugs that impair cardiac ion channel function. Recent experimental and clinical data suggest that LQTS hearts not only demonstrate electrical abnormalities but also exhibit mechanical dysfunction (altered diastolic relaxation and prolonged contraction duration), altered mechanical heterogeneity and impaired electromechanical interaction (electromechanical window), which correlate with the individual's risk for arrhythmia development (Nador *et al.*, 1991; Haugaa *et al.*, 2009; Haugaa *et al.*, 2010; Odening *et al.*, 2013; Lang *et al.*, 2016*a*), and are likely linked to LQT-related arrhythmogenesis (Odening *et al.*, 2022).

In this project, we aimed at characterizing EMC and MEC in rabbits *in vivo* and *ex vivo* in the healthy state and in acquired LQTS (aLQTS).

We chose the rabbit as it mimics human cardiac physiology more closely than smaller lab animals: Rabbit and human hearts share pronounced similarities in ion currents and the shape of action potentials (Nerbonne, 2000), regional systolic and diastolic behavior (Jung *et al.*, 2012) and in MEC mechanisms (Quinn & Kohl, 2016). To exclude a potential impact of chronic electro-mechanical remodeling in inherited LQTS, we utilized an acute, drug-induced LQTS model using the I_{Kr}-blocker E-4031.

Methods

Ethical Approval

All animal experiments were performed in accordance with EU legislation (directive 2010/63/EU) and the German and Swiss animal welfare laws (TierSchG and TierSchVersV), after approval by the animal welfare committee of the local authorities (Regierungspräsidium Freiburg; approval number G18-118; Kanton Bern, Amt für Veterinärwesen, approval number BE115/2019). We confirm that all animal experiments in this study correspond to the journal's animal ethics checklist as outlined in the instructions to authors.

Animal Studies

Adult male and female *New Zealand White* rabbits of similar age and weight were used and obtained from our own breeding at University Hospital Freiburg and from Charles River Laboratories, France. The feeding regime took place according to ad libitum.

For anaesthesia, a bolus of 0.5 ml/kg bodyweight (BW) ketamine S (Ketanest S® 25mg/ml, Pfizer, New York, USA) and 0.2 ml/kg/BW xylazine (Rompun® 2%, Bayer, Leverkusen, Germany) was administered intra-muscularly (IM). This was followed by continuous intravenous (IV) infusion of 1-6ml/h ketamine S / xylazine (titrated by anesthesia-depth) during 12-lead ECG, 24-lead vest ECG and tissue phase mapping cardiac MRI *in vivo*, since this combination does not affect cardiac repolarization (Odening *et al.*, 2008). The depth of anaesthesia was determined by measuring heart and respiratory rate. *Ex vivo* beating heart excision for optical mapping was performed in anaesthetized rabbits after additional injection of 500 IU heparin IV (Heparin-sodium, 25000 IU/ml, Braun, Melsungen, Germany) and euthanasia with 40mg/kg BW thiopental IV (Thiopental-sodium 0.5 g, Inresa, Freiburg, Germany), according to the German and Swiss animal welfare laws and the journals humane euthanasia standards.

12-lead ECG

In vivo conventional 12-lead surface ECGs were performed in rabbits anaesthetized with ketamine S / xylazine as described above (n=13 per group). ECGs were recorded in each rabbit under physiological conditions (control) followed by measurement with I_{Kr}-blocker E-4031 (aLQTS; 10 µg/kg

body weight (BW) bolus; continuous 1 µg/kg BW/min infusion IV). ECGs were performed in both groups – control and aLQTS – at timepoints *baseline* and *peak-preload* (20 sec after the injection of 6ml/kg BW 0.9%-NaCl bolus IV, heated up to body temperature). Instead of conventional QT-interval, RT-intervals were measured to be in line with automated RT-interval annotations in the 24-lead ECG vest (see below). RT-intervals were adjusted to heart beating frequency via calculation of heart rate corrected RTn370 (using $\mathrm{RTn370} = \mathrm{RTobserved} - \left(0{,}22 * \left(\mathrm{RRobserved} - 370\right)\right)\ [ms]$) (Brunner *et al.*, 2008; Ziupa *et al.*, 2019). Temporal heterogeneity of repolarization was parameterized by the short-term variability of RT ($\mathrm{STV_{RT}}\ [\mathrm{ms}] = \sum_{n=1}^{N} \frac{|RT_{n+1} - RT_n|}{(N)^2}$, assessed in 31 consecutive beats) (Baumert *et al.*, 2016). Regional heterogeneity of repolarization was parameterized by RT-dispersion (max-min) ($\mathrm{RTn370} = \mathrm{RTobsverved} - \left(0{,}22 * \left(\mathrm{RRobserved} - 370\right)\right)\ [ms]$, assessed in 6 consecutive beats over 12 leads).

12-lead ECG with pharmacological autonomic blockade

To determine whether the observed mechano-induced electrical changes are (mainly) driven by cardiac-intrinsic mechanisms and not secondary by autonomic reflexes, the same experiments were performed with pharmacological autonomic blockade (n=8 per group)**.** For the pharmacological blockade of sympathetic reflexes, an IV bolus of 0.5ml/kg BW esmolol (Esmolol OrPha®, 2 mg/ml) was administered in rabbits anaesthetized as described above, followed by continuous IV infusion of 1.5ml/kg/h esmolol. For the pharmacological blockade of parasympathetic reflexes, an IM injection of 0.1ml/kg glycopyrronium bromide (Robinul® 0.1 mg/ml) was administered. Both dosages correspond to the recommendations of the VetPharm website for a complete autonomic blockade (www.vetpharm.uzh.ch).
ECGs were recorded continuously at baseline and after bolus injection (20 sec after the injection of 6ml/kg BW 0.9% NaCl bolus IV, heated up to body temperature) and the timepoints *baseline* and *peak-preload* with and without blocker administration were compared. Measurements were performed at two days (day one – with blockers, and day two – without blockers), ensuring the timepoints of measurements matched between conditions.

24-lead ECG vest

Body surface potentials were recorded using a self-fabricated vest in combination with a 24-lead EEG active-electrode ActiveTwo system (BioSemi B.V., Amsterdam, the Netherlands) (Moss *et al.*, 2022). The electrode placement in the vest in relation to the heart position can be seen in Fig. 2F-G and was extracted from previous CT imaging data as described in (Moss *et al.*, 2022). Fig. 2H shows the automated signal annotation of R-peak and T-end that was performed in collaboration with the Karlsruhe Institute of Technology (KIT), Institute of Biomedical Engineering by using the open-source *ECGdeli toolbox for MATLAB* (Pilia *et al.*, 2021) (MATLAB R2019a, The MathWorks, Inc.). 24-lead vest ECGs (vECG) were performed *in vivo* in anaesthetized rabbits (n=6 per group). Recordings were performed at two timepoints, *baseline* and *peak-preload* (20 sec after the injection of 6ml/kg BW

0.9% NaCl bolus IV, heated up to body temperature) in each rabbit under physiological conditions (control) and during E-4031-infusion (aLQTS) (see above). RR-interval, RT-duration, heart rate corrected RTn370-duration and STV_{RT} were assessed. The regional variation of RT-interval was calculated using the following equation: $\mathrm{RT_{difference}(i)\ [ms]} = \mathrm{RTn360(i)} - \min_{I(1\rightarrow 24)} RTn360(i)$, with i being the examined lead and I being the lead with the shortest RT-interval. This enabled the visualization of regional differences in repolarization across the rabbits' torso (Fig. 2I-J).

Tissue phase mapping (TPM-MRI)

To assess regional myocardial longitudinal (Vz) and radial tissue velocities (Vr), rabbits anaesthetized with ketamine S / xylazine (as described above, n=19 per group) were subjected to TPM-MRI in a 1.5T MR machine (Avanto, Siemens, Germany) with high temporal (7.6 ms) and spatial resolution (1.0 x 1.2 x 4 mm) (further described in Jung *et al.*, 2012; Odening *et al.*, 2013). Systolic and diastolic velocities were acquired in each rabbit under physiological conditions (control) and during E-4031 infusion (aLQTS) (see above). Systolic and diastolic peak velocities (AMPsys and AMPdia, respectively) as well as *time-to-diastolic peak* duration (TTPdia), a marker for contraction duration (Odening *et al.*, 2013; Ziupa *et al.*, 2019), were derived from left ventricular (LV) tissue velocity curves in both longitudinal (Vz) and radial (Vr) directions (Fig. 3A-D). To this end, the LV was partitioned into 16 segments in the base, mid and apex (modified American Heart Association model) (Cerqueira *et al.*, 2002). As *time-to-diastolic peak* duration is heart rate dependent, but an accurate heart rate correction formula has not yet been defined, we measured and compared *time-to diastolic peak* only in rabbits with similar RR-interval duration in control and aLQTS measurements (n=9). Data processing was accomplished by using a customized MATLAB software.

Langendorff-perfusion of rabbit hearts

Rabbits were anaesthetized with ketamine S / xylazine (12.5/3.75 mg/kg) IM and were administered 1000 IU heparin IV via ear vein injection (n=6). Following euthanasia with thiopental-sodium IV (40 mg/kg body weight), the heart was rapidly excised, and cannulated on a modified Langendorff perfusion system (Hugo Sachs). The heart was perfused with modified Krebs-Henseleit (KH) solution at constant pressure (80 mmHg) (Hornyik *et al.*, 2020). Aortic pressure, flow rate, and temperature were monitored and a pseudo-ECG (monopolar Ag/AgCl pellet electrodes in the solution near the cardiac surface) was recorded.

A modified version of the Langendorff-perfused heart set-up was used to study MEC *ex vivo*. In this 'working-heart-like' configuration, a latex balloon was placed into the left ventricle (LV) and was used to set different end-diastolic LV pressure levels to mimic different preloads. The balloon was filled with KH solution and was connected via tubes to a water column (in a calibrated cylinder). The calibrated cylinder was positioned at different heights relative to the heart, thereby providing the desired preload levels (0, 6, 15 mmHg), while enabling 'free' contraction of the LV (hence the term: 'working-heart-like' configuration).

Panoramic optical mapping of beating hearts

A combined Langendorff and optical mapping (OM) setup was used to study regional heterogeneities in electrical (action potential) characteristics and mechano-electrical interactions *ex vivo* (Fig. 1). A three-view mirror-based panoramic OM system was used with healthy and aLQTS hearts (n=6 per group). Acquired LQTS was obtained by adding 50 nM E-4031 into the KH solution to inhibit I_{Kr}-channels after the baseline measurements, and perfusion was maintained for at least 10 min before action potential duration (APD) measurements were started. Voltage-sensitive dye (Di-4-ANBDQPQ, Cytocybernetics, Buffalo, NY, USA) was injected directly into the aortic root for coronary perfusion (20 µL of 8.6 mM injected in 0.5 µL increments over 5 minutes). The hearts were paced at 2.5 Hz with an electrical stimulator on the left atrium to maintain a normal ventricular activation via an intact conduction system. In contrast to the standard OM approach, *no* pharmacological motion uncoupler agent (e.g., blebbistatin) was applied to maintain normal mechanical contraction. The three cardiac views were projected with mirrors onto one sCMOS camera (Andor Zyla 5.5, Oxford Instruments, UK) recording at a frame rate of 200 Hz. Multiple red light-emitting diodes (LED CBT-90-RX/B, Luminus Devices, Inc. Sunnyvale, CA; filter: ZET642/20X; Chroma) were used for excitation. Fluorescence emission was collected via a high-speed lens (DO-5095, Navitar) and a custom emission filter (ET585/50M+800/200M, Chroma).

MEC was studied both in healthy and aLQTS hearts by detecting changes in electrical characteristics (ECG and action potential parameters) following rapid alterations in mechanical function by changing LV preload (preloads: 6 – 0 – 15 – 6 mmHg). For analysis of fluorescence signals, the acquired files were cropped to ensure that each recording starts at diastole and the recordings were averaged across multiple heart beats to obtain an optical recording of a single action potential with a high signal-to-noise ratio.

Following beat averaging, motion correction of the resulting OM signals was used to separate motion-induced and voltage-induced changes in fluorescence of the beating hearts. A published sub-pixel image registration approach was used to track changes between an image of the heart in diastole (base image) and during contraction (HajiRassouliha *et al.*, 2017, HajiRassouliha *et al.,* 2018). Sub-image sizes of 32 pixels were used with step sizes of 20 pixel (CC32SS20) to find the tracked points between images. These were used to predict the location of each pixel from the base image on each of the tracked images. The intensity value at each of these locations was then estimated by interpolating between pixels in the image being motion corrected. The resulting intensities formed the motion corrected image. Subsequently, the data was analyzed with a custom-made MATLAB (Mathworks) program for OM analysis (available from the authors on request). For this purpose, the signals were normalized and inverted, and regions of interest (ROIs) – 10x10 pixel size (2.6x2.6mm) – were defined as follows: LV base (ROI 1), mid (ROI 2), and apex – anterior view; RV base (ROI 3) and LV base (ROI 4) – left-posterior view; RV mid (ROI 5) – right-lateral view.

Statistical analysis

Statistical analysis was performed using *GraphPad Prism 8* (GraphPad Software, San Diego, USA). Data are expressed as means ± standard deviation. Comparison of control and aLQTS rabbits was performed using paired Student's *t* test, significance was established at $p<0.05$. The n value reflects the number of rabbits used per group (e.g., n=13 per group, that is 13 control and 13 aLQTS animals).

Results

Alteration of cardiac repolarization in acquired LQTS in vivo

Prolongation of heart rate corrected RT-interval

12-lead surface ECG (Fig. 2A) demonstrated a prolongation of cardiac repolarization during the infusion of I_{Kr}-blocker E-4031 (aLQTS) in all individual animals (Fig. 2B). The RT-interval prolonged (control 163.85 ± 18.54 ms vs. aLQTS 194.69 ± 25.34 ms, $p<0.0001$, n=13 per group), while the RR-intervals slightly decreased (e.g., heart rates increased) (control 402.39 ± 55.56 ms vs. aLQTS 373.23 ± 47.00 ms, $p=0.021$, n=13 per group), leading to a pronounced prolongation of heart rate corrected RTn370-interval in aLQTS (control 156.61 ± 11.59 ms vs. aLQTS 193.95 ± 19.60 ms, $p<0.0001$, n=13 per group) (Fig. 2B).

Increased temporal and regional heterogeneity of repolarization

To elucidate ECG parameters indicative of an increased pro-arrhythmic risk in aLQTS, temporal and regional heterogeneity of repolarization were assessed. Short-term variability of RT (STV_{RT}) – a marker for temporal heterogeneity of repolarization – was significantly increased in aLQTS compared to control (Fig. 2C). Similarly, RT-dispersion (max-min) – a marker for regional heterogeneity of repolarization – was increased significantly during the infusion with I_{Kr}-blocker E4031 (Fig. 2D).

The calculation of the deviation of the individual RT from the shortest RT in the vECG enabled a visualization of the regional variation of RT-interval ($RT_{difference}$) projected on the rabbits' thoraces. While in the LV basal region no remarkable differences were apparent in the pattern of regional RT-interval variation between both groups, RTn370 increased in the apical region in aLQTS compared to control, with significant increase in $RT_{difference}$ in lead 21 and 22 (as indicated by the higher color-gradient; lead 21, $p=0.004$, lead 22, $p=0.041$, n=5 per group) (Fig. 2I-J). Moreover, in aLQTS the change in regional RT-interval was visually noticeable in the leads depicting the right ventricle (lead 10, 15, 17, 23) with particularly pronounced changes in RTdifference (indicated in red in Fig. 2I-J) in 4 out of 6 animals. In these, the RV-LV difference was 3.46 ± 1.73 ms in control and increased to 9.09 ± 5.28 ms in aLQTS ($p=0.13$, paired t-test, Fig. 2 E,I,J).

Induction of mechanical alterations via EMC in vivo

Using tissue-phase mapping MRI, which allows a detailed analysis of regional cardiac function, the effect of electrical changes (e.g., prolongation of cardiac repolarization in aLQTS) on mechanical features was assessed.

Myocardial systolic and diastolic velocities

Peak systolic (AMPsys) and diastolic (AMPdia) tissue velocities in radial (Vr) and longitudinal (Vz) direction were compared between control and aLQTS. In line with a prolongation of cardiac repolarization, E-4031 infusion increased systolic peak velocities in 1 out of 16 longitudinal (Vz AMPsys, n=19 per group) and 5 out of 16 radial (Vr AMPsys, n=19 per group) LV segments, indicating an improved systolic function (Table 1). While radial diastolic peak velocities (Vr AMPdia) remained unchanged, longitudinal diastolic peak velocities (Vz AMPdia) were significantly decreased in 6/6 basal and 4/6 mid segments in aLQTS compared to control (Fig. 3B), suggesting an E-4031-induced diastolic dysfunction via EMC.

Table 1. E-4031 induced changes in systolic tissue velocity (Vz AMPsys, Vr AMPsys)

		control (n=19)		aLQTS (n=19)		student's t-test
Vz AMPsys (cm/s)		Mean	SD	Mean	SD	
Apex	septal	1.83	1.11	2.53	1.33	p=0.0042
Vr AMPsys (cm/s)						
Mid	anterior	1.78	0.27	2.02	0.48	p=0.0224
	anterolateral	1.67	0.34	1.90	0.44	p=0.0186
Apex	anterior	1.23	0.29	1.50	0.38	p=0.0223
	lateral	1.27	0.39	1.55	0.40	p=0.0233
	septal	1.34	0.25	1.69	0.55	p=0.0051

Time-to-diastolic peak

Time-to-diastolic peak duration, a marker for the duration of contraction and early relaxation, was significantly prolonged in 9/16 segments in longitudinal (Vz, Fig. 3C) and 3/16 segments in radial (Vr) directions (Vr, Table 2) of the rabbits' LV in aLQTS as compared to control.

Table 2. E-4031 induced changes in radial diastolic contraction duration (Vr TTPdia)

		control (n=9)		aLQTS (n=9)		student's t-test
Vr TTPdia (ms)		Mean	SD	Mean	SD	
base	anterolateral	220.82	30.43	229.27	39.49	p=0.0208
	Inferolateral	210.69	26.54	229.27	35.44	p=0.0286
Mid	inferior	234.33	22.80	247.84	26.72	p=0.0145

Apico-basal heterogeneity in mechanical function

To investigate the impact of the increased repolarization heterogeneity in aLQTS on regional mechanical heterogeneity, we calculated apico-basal heterogeneity – defined as difference between all basal and all apical values. In aLQTS, apico-basal heterogeneity in longitudinal diastolic peak velocities (Vz AMPdia) showed a significant decrease compared to control (control -4.34 ± 1.19 cm/s vs. aLQTS -3.18 ± 1.19 cm/s, p=0.0008, n=17 per group) (Fig. 3E). In contrast, apico-basal heterogeneity in longitudinal *time-to-diastolic peak* duration (Vz TTPdia) was significantly increased in aLQTS compared to control (control 4.16 ± 8.82 ms vs. aLQTS 20.54 ± 10.31 ms, p=0.037, n=8 per group) (Fig. 3F), indicating an impact of electrical changes also on mechanical heterogeneity.

Mechano-induced changes in electrical (dys-)function via MEC in vivo

In surface ECG-measurements, alterations in mechanical function (via increased preload) resulted in changes of electrical function via MEC.

Mechano-induced changes in RR and RT intervals

RT-intervals prolonged and heart rate increased (i.e., RR-intervals shortened) after acute 0.9%-NaCl IV bolus application under physiological conditions (control) and with I_{Kr}-blocker E-4031 (aLQTS) (Fig. 4A). Heart rate changes did not differ significantly between control and aLQTS groups. Heart rate corrected RTn370-intervals prolonged in both groups (Fig. 4 B.2). Interestingly, RTn370-prolongation was significantly more pronounced in aLQTS compared to control (p=0.0056, n=13 per group) (Fig. 4 B.2), indicating that cardiac repolarization in aLQTS may be more susceptible to acute MEC effects than in healthy (control) hearts.

Arterial blood pressure was measured in both groups at *baseline* (15 sec before increase in preload) and at the time of the maximal RTn370 increase (around 20 sec after NaCl bolus injection) in n=5 rabbits. Mean arterial blood pressure (MAP) decreased significantly in both groups following bolus injection (in the range of 6-8 mmHg) (Fig. 5 A.1). Importantly, the delta between *baseline* and *RTn370-peak* (Δ*peak-baseline*) showed no significant difference between control and aLQTS (Fig. 5 A.2).

To further investigate whether the observed changes in the electrical function (RT) are mainly due to intrinsic mechano-induced electrical changes or whether (some parts of it) are mediated secondarily by autonomic reflexes, we performed additional experiments in a subset of control rabbits before and after complete blockade of the parasympathetic and sympathetic system. Heart rate measurements were performed to validate the pharmacological autonomic blockade. While no changes in heart rate were observed due to betablockade alone – likely due to parasympathetic predominance in rabbits anaesthetized with xylazine and the consecutive slow heart rate – we observed an increase in heart rate after the parasympathetic blocker was also added (Fig. 5B.3). In these experiments, the bolus-induced changes in RTn370 did not differ between baseline and autonomic-blockade experiments (Fig. 5B), suggesting a direct role of myocardial stretch caused by increased preload on the observed electrical alterations.

Mechano-induced changes in heterogeneity of repolarization

In 12-lead surface ECG, the increase in preload under physiological conditions (control) resulted in a significant increase in temporal heterogeneity, so called STV_{RT}, exemplarily seen in Fig. 4C. In aLQTS, in which the *baseline* STV_{RT} was already pronouncedly higher than in controls, there was no significant increase in STV_{RT} from *baseline* to *peak-preload* (Table 3). Regional RT-dispersion (max-min) from baseline to peak was only increased significantly in aLQTS and showed no significant change in healthy rabbit hearts (Table 3).

Table 3. Mechano-induced changes in heterogeneity of repolarization

	control			aLQTS		
	baseline (n=13)	peak-preload (n=13)	student's t-test	baseline (n=13)	peak-preload (n=13)	student's t-test
STV_{RT} (ms)	3.45 ± 1.03	4.84 ± 1.69	p=0.0254	5.25 ± 1.69	6.09 ± 2.15	ns (p=0.28)
RT-dispersion (max-min) (ms)	21.41 ± 5.73	25.83 ± 5.76	ns (p=0.13)	25.83 ± 5.76	32.69 ± 12.79	p=0.0256
Data are presented as mean ± SD.						

The pattern in regional RT-heterogeneity obtained from the 24-lead ECG vest recordings in n=6 rabbits per group changed with increased preload. Regional variation of the individual RT from the shortest RT ($RT_{difference}$) in healthy control revealed only slight changes in leads 10, 15-17 and 23 picturing the RV regions (Fig. 4D), and standard deviation of $RT_{difference}$ over all 24 leads – depicting regional RT-heterogeneity – remained almost the same (control *baseline* SD 2.86 ms vs. control *peak* 2.54 ms). In aLQTS, although there was no significant change in overall mean $RT_{difference}$ between *baseline* and *peak-preload* (aLQTS *baseline* 8.59±4.25 vs. aLQTS *peak* 9.28±2.78 ms, p=0.29).

In summary, increased preload-mediated RT-prolongation and RT-heterogeneity altering effects were more pronounced in E-4031-induced aLQTS hearts, indicating that cardiac repolarization in LQTS may be more susceptible to acute MEC effects than in healthy hearts.

Investigations of MEC ex vivo in Langendorff-perfused hearts

We developed the above described Langendorff-perfused 'working-heart-like' OM setup, with the idea of investigating MEC on the *ex vivo* whole heart level through direct control of the preload. This, in turn, should provide us with a tool for future testing of the potential role of different stretch-activated channels on mechano-electrical interactions.

Alteration of cardiac repolarization in acquired LQTS hearts ex vivo

The application of E-4031 (50 nM) resulted in significantly prolonged QT intervals in the *ex vivo* ECG and lengthened LV action potential durations (APD) detected by OM (Fig. 6A-B). The RV APDs tended to increase similarly with E-4031 (Fig. 6B). However, due to pronounced motion artefacts in the RV, the APDs at RV mid could be investigated only in a subset of the hearts (n=2). Physiological apicobasal difference in LV APD could be observed in control (APD75 at LV apex vs. LV mid [ms±SD]: 115.0±17.4 vs. 121.4±14.6, p=0.05, n=6; Fig. 6B). Interestingly, this regional heterogeneity in electrical function was not further increased in aLQTS (ΔAPD75 (LV mid - LV apex) [ms±SD]: control 6.4±6.2 vs. aLQTS 6.2±7.0, p=0.9382, n=6).

Mechano-electrical coupling (MEC) ex vivo

As shown in Fig. 6 C.1, unfortunately, no mechano-induced global electrical change could be detected by our model: neither decreased (from 6 to 0 or 15 to 6 mmHg) nor increased (from 0 to 15 or 0 to 30 mmHg) preload induced any change in QT intervals at any measured time points. We could not detect any mechano-induced changes in APD (Fig. 6 C.2). While mechano-induced changes in duration and/or regional heterogeneity of APD may have occurred in our model; the OM APD measurement in the beating heart was limited due to inaccuracies of the used motion tracking approach at different preloads, during which contractility and consecutive motion artifacts changed.

Discussion

In this study, we systematically assessed electromechanical reciprocity in healthy and E-4031-induced acquired LQTS (aLQTS) rabbit hearts to identify EMC and MEC as drivers of (potentially pro-arrhythmic) electro-mechanical heterogeneity. We confirmed previous observations on EMC in LQTS: electrical alterations (e.g., prolongation and increased dispersion of repolarization) in aLQTS led to decreased diastolic function and prolonged contraction duration and – importantly – changed left-ventricular mechanical heterogeneity. Moreover, we demonstrated the presence of MEC in the healthy and aLQTS heart: an acute increase in mechanical preload led to a prolongation of heart rate corrected RT-interval in both healthy and – even more – in aLQTS rabbit hearts. Additionally, we revealed a mechano-induced increase in regional RT-dispersion and alterations in the pattern of RT-heterogeneity in aLQTS.

Altered electrical heterogeneity in acquired LQTS

The measurement of electrical heterogeneity in repolarization and its deviation from a physiological magnitude is an acknowledged instrument to (indirectly) assess cardiac arrhythmogenicity (Baumert *et al.*, 2016). We confirmed that in aLQTS rabbit hearts, short-term variability of RT (STV_{RT}) – a marker for temporal heterogeneity of repolarization – as well as RT-dispersion (max-min) – a marker for regional heterogeneity of repolarization – were increased significantly, which is consistent with previous findings in human subjects (Napolitano *et al.*, 2000; Hinterseer *et al.*, 2009). This increase in electrical heterogeneity is presumably caused by the heterogenous distribution of I_{Kr} conducting hERG potassium channel. The LV apex shows a three times higher amount of hERG channel than the LV base in rabbit heart tissue (Cheng *et al.*, 1999). As 12-lead ECG RT-dispersion only allows an assumption of changes in electrical heterogeneity but does not provide information about the actual regional differences, e.g., apico-basal and RV-LV heterogeneity, we designed a self-fabricated 24-lead ECG vest, enabling us to visualize acute changes in $RT_{difference}$ on the rabbits' thoraces. And indeed, using this new method, we were able to detect significant apical $RT_{difference}$ prolongation by I_{Kr}-blocker E-4031, leading to altered electrical heterogeneity in aLQTS. Also in right cardiac regions, RT-heterogeneity was altered in aLQTS compared to healthy controls. These results stand in line with novel findings in ECGI – a noninvasive method depicting regional differences in the activation-recovery interval (ARI), a surrogate for APD (Vijayakumar *et al.*, 2014), with 224-multielectrode body-surface ECG in combination with CT-based reconstruction on the human heart (Rudy & Burnes, 1999; Rudy, 2017). In ECGI, patients with congenital LQTS type 2 (LQT2; loss-of-function mutations in KCNH2/hERG with reduction of I_{Kr} (Schwartz *et al.*, 2012)) showed overall spatially heterogenous activation-recovery intervals and steeper repolarization gradients than in healthy controls (Vijayakumar *et al.*, 2014). Importantly ARI were strongly prolonged in RV regions in LQT2 compared to control, resulting in a much steeper gradient of repolarization across the border of LV and RV (Vijayakumar *et al.*, 2014), similarly as in our vECG in aLQTS. As the acute induction of aLQTS showed comparable effects on regional repolarization pattern as genetic 'chronic' LQTS, this could either suggest that remodeling in chronical disease might be minimal – or that acute, I_{Kr}-blocker induced electrical changes just further progress in genetic LQTS.

Altered mechanical heterogeneity in acquired LQTS

Substantiating the mounting evidence that LQTS is an 'electro-mechanical' – rather than a 'purely electrical' – disease, we observed impaired diastolic peak velocities (AMPdia) in longitudinal direction (Vz) in the overall base and 4/6 mid segments and significantly prolonged *time-to-diastolic peak* duration (TTPdia), a marker for contraction duration. Moreover, we complemented these data with a novel aspect by revealing significant EMC-induced changes in apico-basal heterogeneity in Vz AMPdia and Vz TTPdia.

Our findings regarding the AMPdia and TTPdia are in line with our previous studies, in which longitudinal diastolic peak velocities were more affected than radial velocities in drug-induced aLQT2 (Odening *et al.*, 2013; Ziupa *et al.*, 2019), while in congenital LQT2 rabbit hearts longitudinal and radial velocities were similarly affected (Odening *et al.*, 2013). The impact of E-4031 on mechanical function, however, was substantially more pronounced in our study compared to Ziupa et al.'s work in 2019 (Ziupa *et al.*, 2019). Sex differences in the rabbits' cohorts might be the possible explanation. While Ziupa et al. examined exclusively male animals (Ziupa *et al.*, 2019), we investigated a sex-mixed cohort, mainly consisting of female rabbits. Testosterone is known to increase I_{Kr} and I_{Ks}, making male hearts less prone to I_{Kr}-blocker induced or congenital QT prolongation than female hearts (reviewed in (Odening & Koren, 2014)). In transgenic LQT2 rabbits, Lang et al. (Lang *et al.*, 2016*b*) observed that female animals exhibit a prolonged TTPdia compared to males, indicating that the impact of I_{Kr}-blocker E-4031 on mechanics might be similarly more pronounced in female rabbits, leading to a potentially higher pro-arrhythmic risk in female subjects due to more prominent electrical *and* mechanical changes in aLQTS.

Accordingly, we revealed pronounced alterations of mechanical dispersion in aLQTS with decreased apico-basal heterogeneity in diastolic peak velocities and increased apico-basal heterogeneity in contraction duration. Similarly to our findings, Brado et al. (Brado *et al.*, 2017) described an altered apico-basal longitudinal relaxation sequence in pediatric patients with genetic LQTS in TPM-MRI. In tissue doppler (Haugaa *et al.*, 2010; Borowiec *et al.*, 2020) and strain (Haugaa *et al.*, 2009; ter Bekke *et al.*, 2015) echocardiography, comparable alterations in mechanical function have been observed in LQTS. Transmural and apico-basal alteration in mechanical relaxation, prolonged contraction duration and the so called electromechanical window negativity (ter Bekke *et al.*, 2015) – describing the abnormal closure of the aortic valve before the end of the prolonged electrical repolarization – have been reported. Importantly, regional differences in mechanical dysfunction have been linked to arrhythmic risk, with longer apical radial strain in symptomatic than in asymptomatic LQTS patients (Borowiec *et al.*, 2020), underlining the importance of a better understanding of mechanical heterogeneity in aLQTS-related arrhythmogenesis.

Mechano-electrical coupling in healthy and aLQTS rabbit hearts

Mechanically-induced changes in electrical function occur frequently, both in healthy and diseased hearts, for example due to volume or pressure overload (Quinn & Kohl, 2021), Valsalva maneuver (Taggart *et al.*, 1992), local endocardial contact caused by intracardiac devices such as catheters

(Befeler, 1978; Quinn & Kohl, 2021) or due to extra-thoracal applied forces, such as *commotio cordis* (Quinn & Kohl, 2021).

In this study, we revealed a prolongation of repolarization duration (heart rate corrected RTn370-intervals) upon an increase in preload in healthy and aLQTS hearts. Importantly, these mechano-induced electrical changes, e.g., RT prolongation and increased heterogeneity, were particularly pronounced in aLQTS with already pre-existing prolongation of cardiac repolarization, suggesting that these hearts may be particularly prone to MEC.

Mechanically-induced electrical changes are timing-dependent (Quinn & Kohl, 2021), e.g., can lead to APD prolongation or shortening depending on the occurrence in relation to the cardiac cycle, and may – under physiological conditions – be part of regional synchronization of ventricular repolarization (Opthof *et al.*, 2015; Quinn & Kohl, 2021). Over the entire cardiac cycle, the increase in mechanical preload can affect APD, ventricular refractoriness and conduction (Quinn & Kohl, 2021). In our study, we recorded a significant prolongation in cardiac repolarization in healthy and aLQTS hearts consistently around 20 seconds after the IV bolus. This prolongation occurred to a similar extent with intact autonomic activity and after pharmacological blockade of both the sympathetic and parasympathetic nervous system, suggesting that this mechano-induced electrical alteration is not solely due to autonomic modulation / reflex loops, but may indeed be caused by cardiac-intrinsic mechanisms such as electrical alterations caused by bolus-induced changes in myocardial stretch, or a combination of both.

Of note, considering that xylazine increases the parasympathetic tone, our anaesthetic regimen might not be ideal in the setting of investigating the effect of pharmacological autonomic blockade on MEC. However, as we are interested in changes in cardiac repolarization, and it is shown that the ketamine/xylazine combination has no effect on cardiac repolarizing ion currents (Odening *et al.*, 2008), it is of advantage to utilize this regimen as opposed to the alternative options such as propofol or isoflurane, which do block various repolarizing ion channels.

Importantly, the mechano-induced electrical alterations were particularly pronounced in aLQTS, in which not only an overall RT prolongation occurred, but also an increase in regional RT-dispersion in 12-lead ECG and a changed pattern of RT heterogeneity. These data indicate that acute changes in (global) myocardial stretch may cause additional alterations of electrical function in aLQTS. When these changes exert regionally divergent effects – as observed in our study in aLQTS – they may potentially increase proarrhythmic APD heterogeneity and thereby facilitate arrhythmia formation in acquired QT-prolongation. However, no direct evidence was provided in our rabbit model on whether these alterations in the electrical function can further evolve into arrhythmias. There are several reasons that may account for the lack of arrhythmic events in our acute drug-induced LQTS model. Not only is the I_{Kr}-blocker E-4031 a short acting drug, but we also monitor the rabbits for a short period of time and have only performed one single change in preload during 12-lead ECG and one during vECG in each aLQTS animal, which might be too little to observe ME-induced arrhythmic events. Moreover, the rabbits are also under anaesthesia with ketamine/xylazine during the ME interventions, which may further contribute to a lack of arrhythmic events due to an overall relatively low sympathetic tone with parasympathetic predominance.

Along the lines of the concept of a 'sensitized' cardiac tissue in LQTS due to the disproportional prolongation of cardiac repolarization compared to the less pronounced prolongation of contraction duration (Odening *et al.*, 2022), e.g., the negative electro-mechanical window (ter Bekke *et al.*,

2015), our findings indicate that cardiac repolarization in aLQTS may be more susceptible to acute MEC effects than healthy hearts. These effects are likely to be exaggerated with rapid mechanical alterations, particularly if the mechanical alterations occur in the later phase of the electromechanical window, in which mechanical systole is already completed, while the electrical repolarization is still ongoing (Odening *et al.*, 2022).

Whether this apparently increased mechano-sensitivity in LQTS is mainly because a longer cardiac repolarization is in general more prone to additional QT-prolongations – the paradigm of an "intrinsic" APD-dependence of APD-modulation (Zaza, 2016; Winter & Shattock, 2016) – or whether the LQTS / aLQTS heart has an intrinsically increased mechano-sensitivity remains to be investigated. The molecular mechanism behind MEC is postulated to be based on an interplay between intracellular Ca^{2+}-concentration and -sensitivity, and mechano-sensitive channels (MSCs) (Quinn & Kohl, 2021). MSCs are a group of channels that can either be directly activated by stretch (stretch-activated channels, SACs) or channels that are mainly voltage- or ligand-gated but exhibit a certain degree of mechano-sensitivity (e.g. I_{CaL}, I_{Ks}, I_{Na} und I_{KATP}) (Sachs, 2009). While non-selective SACs (SAC_{NS}) can cause depolarization and excitation in resting cells, they can accelerate early repolarization and APD-shortening during the plateau phase or prolong APD when activated later during repolarization (Quinn & Kohl, 2021). Therefore, SAC_{NS} could explain most of the observed mechano-induced electrical alterations; but, it remains to be demonstrated whether these channels are the main determinant of MEC in the whole heart (Quinn & Kohl, 2021).

To provide a framework, in which the potential impact of different SACs as mediators of mechano-induced RT/APD prolongation could be investigated in the future, we aimed to establish an OM setup with a beating rabbit heart, in which the preload can be changed and resulting changes in global and regional action potential duration can be measured. We developed the above described Langendorff-perfused 'working-heart-like' OM setup and could identify E-4031-induced APD-prolongation in beating hearts at the physiological 6 mmHg preload using our motion-correction tool. We were, however, facing several problems in accurately determining APD when increasing preload, which resulted in stronger contraction. The motion tracking approach could correct for in-plane motion, particularly in the center of the field-of-view, however out-of-plane motion (i.e., towards or away from the camera) could not be corrected for and caused significant artifacts in the recorded signals. This precluded any consistent assessment of potential APD-changes with changed preload. However, even in the *ex vivo* surface ECG, no RT-changes were observed with changed preloads, suggesting that also the method of setting different preloads might need further improvement.

Several technical limitations of our current OM "pseudo-beating-heart-like" setup could be improved in the future: 1) Changing to a 4-view configuration would allow better surface tracking (due to higher overlap of the different cardiac views), better motion correction, and thereby, less disturbed 'corrected' voltage-signals. 2) Adding telecentric illumination to have less changes in light intensity with distance to the LED to improve signal quality with out-of-plane motion. 3) Taking advantage of ratiometric potentiometric dyes to further reduce motion artifacts. 4) Implementing a more physiological 'working-heart' model would enable better control of preload and could result in more physiological mechanical function. 5) Placing a second balloon into the RV would reduce rotational

motion and would represent a more physiological setting, in which the preload of both ventricles could be changed and both, simultaneous preload-changes as well as acute RV-LV heterogeneities in preload could be investigated. We are currently implementing these modifications, with the aim to obtain more accurate and regionally detailed AP signals. This will hopefully allow us to detect more subtle MEC-induced changes in APD and its heterogeneity, as well as to test the impact of activation and/or blockade of various SAC on MEC.

Conclusion

We observed mechano-induced prolongation of cardiac repolarization both in healthy and aLQTS rabbit hearts. Importantly, this mechano-induced prolongation and increased heterogeneity in repolarization was more pronounced in the aLQTS setting, suggesting that acute MEC effects may play an additional role in LQT-related arrhythmogenesis. Further mechanistic studies are needed to fully understand the extent of MEC in aLQTS and the underlying drivers. To this end, a further optimization of the here introduced panoramic 'beating-heart' OM system and the approach to implement preload changes is warranted.

Additional information section

Data availability statement

All data will be made available upon reasonable request to the corresponding author.

Competing interests

The authors declare that they have no known competing financial interests that could have appeared to influence the work reported in this paper.

Author contributions

RDL, SN, NA, TH, MM, SJ, TPW, GS, CMZJ, RL, KEO concepted and designed the experiments. RDL, SN, NA, MM, TH, SJ, RM, SPF performed the experiments. RDL, SN, NA, TH, SJ, NP, KEO analyzed and interpreted the data. RDL, SN, NA, TH, KEO wrote the manuscript, with critical review by all authors (SJ, RM, MM, NP, TPW, AH, MZ, GS). All authors approved the final version of the manuscript and agreed to be accountable for all aspects of the work. All persons designated as authors qualify for authorship, and all those who qualify for authorship are listed.

Funding Sources

German Research Foundation (DFG) Project #*394630089* to K.E.O. and G.S.
Swiss National Science Foundation SNF grant 310030_197595 to K.E.O

C.M. Z.i-J. is a member of SFB1425, funded by DFG – Project #422681845

Keywords

Electromechanical reciprocity, Electro-mechanical dysfunction, Cardiac electrophysiology, I_{Kr}, Long QT syndrome, ECG imaging

Permission and use of previously published material

References

Antzelevitch C & Fish J (2001). Electrical heterogeneity within the ventricular wall. *Basic Res Cardiol* **96,** 517–527.

Baumert M, Porta A, Vos MA, Malik M, Couderc J-P, Laguna P, Piccirillo G, Smith GL, Tereshchenko LG & Volders PGA (2016). QT interval variability in body surface ECG: measurement, physiological basis, and clinical value: position statement and consensus guidance endorsed by the European Heart Rhythm Association jointly with the ESC Working Group on Cardiac Cellular Electrophysiology. *Europace* **18,** 925–944.

Befeler B (1978). Mechanical stimulation of the heart: its therapeutic value in tachyarrhythmias. *Chest* **73,** 832–838.

ter Bekke RMA, Haugaa KH, van den Wijngaard A, Bos JM, Ackerman MJ, Edvardsen T & Volders PGA (2015). Electromechanical window negativity in genotyped long-QT syndrome patients: relation to arrhythmia risk. *European Heart Journal* **36,** 179–186.

Borowiec K, Kowalski M, Kumor M, Duliban J, Śmigielski W, Hoffman P & Biernacka EK (2020). Prolonged left ventricular contraction duration in apical segments as a marker of arrhythmic risk in patients with long QT syndrome. *EP Europace* **22,** 1279–1286.

Brado J, Dechant MJ, Menza M, Komancsek A, Lang CN, Bugger H, Foell D, Jung BA, Stiller B, Bode C & Odening KE (2017). Phase-contrast magnet resonance imaging reveals regional, transmural, and base-to-apex dispersion of mechanical dysfunction in patients with long QT syndrome. *Heart Rhythm* **14,** 1388–1397.

Brunner M et al. (2008). Mechanisms of cardiac arrhythmias and sudden death in transgenic rabbits with long QT syndrome. *J Clin Invest*. **118**, 2246-59.

Cerqueira MD, Weissman NJ, Dilszian V, Jacobs AK, Kaul S, Laskey WK, Pennell DJ, Rumberger JA, Ryan T & Verani MS (2002). Standardized Myocardial Segmentation and Nomenclature for Tomographic Imaging of the Heart. *Circulation*. **105**, 539-42.

Cheng J, Kamiya K, Liu W, Tsuji Y, Toyama J & Kodama I (1999). Heterogeneous distribution of the two components of delayed rectifier K+ current: a potential mechanism of the proarrhythmic effects of methanesulfonanilideclass III agents. *Cardiovascular Research* **43,** 135–147.

HajiRassouliha A, Taberner AJ, Nash MP & Nielsen PMF (2017). Motion Correction Using Subpixel Image Registration. In *Reconstruction, Segmentation, and Analysis of Medical Images*, pp. 14–23. Springer International Publishing, Cham.

HajiRassouliha A, Taberner AJ, Nash MP & Nielsen PMF (2018). Subpixel phase-based image registration using Savitzky–Golay differentiators in gradient-correlation. *Computer Vision and Image Understanding* **170,** 28–39.

Haugaa KH, Edvardsen T, Leren TP, Gran JM, Smiseth OA & Amlie JP (2009). Left ventricular mechanical dispersion by tissue Doppler imaging: a novel approach for identifying high-risk individuals with long QT syndrome. *Eur Heart J* **30,** 330–337.

Haugaa KH, Amlie JP., Berge KE, Leren TP., Smiseth OA., & Edvardsen T (2010). Transmural Differences in Myocardial Contraction in Long-QT Syndrome. *Circulation* **122,** 1355–1363.

Hinterseer M, Beckmann BM, Thomsen MB, Pfeufer A, Dalla Pozza R, Loeff M, Netz H, Steinbeck G, Vos MA & Kääb S (2009). Relation of increased short-term variability of QT interval to congenital long-QT syndrome. *Am J Cardiol* **103,** 1244–1248.

Hornyik T, Castiglione A, Franke G, Perez-Feliz S, Major P, Hiripi L, Koren G, Bősze Z, Varró A, Zehender M, Brunner M, Bode C, Baczkó I & Odening KE (2020). Transgenic LQT2, LQT5, and LQT2-5 rabbit models with decreased repolarisation reserve for prediction of drug-induced ventricular arrhythmias. *Br J Pharmacol* **177,** 3744–3759.

Janse MJ, Coronel R, Opthof T, Sosunov EA, Anyukhovsky EP & Rosen MR (2012). Repolarization gradients in the intact heart: transmural or apico-basal? *Prog Biophys Mol Biol* **109,** 6–15.

Jung BA, Odening KE, Dall'Armellina E, Föll D & Schneider JE (2012). A comprehensive quantitative comparison of myocardial motion in mice, rabbits and humans using phase contrast MRI. *J Cardiovasc Magn Reson* **14,** P54.

Lang CN, Koren G & Odening KE (2016*a*). Transgenic rabbit models to investigate the cardiac ion channel disease long QT syndrome. *Prog Biophys Mol Biol* **121,** 142–156.

Lang CN, Menza M, Jochem S, Franke G, Perez Feliz S, Brunner M, Koren G, Zehender M, Bugger H, Jung BA, Foell D, Bode C & Odening KE (2016*b*). Electro-mechanical dysfunction in long QT syndrome: Role for arrhythmogenic risk prediction and modulation by sex and sex hormones. *Progress in Biophysics and Molecular Biology* **120,** 255–269.

Moss R, Wülfers EM, Lewetag R, Hornyik T, Perez-Feliz S, Strohbach T, Menza M, Krafft A, Odening KE & Seemann G (2022). A computational model of rabbit geometry and ECG: Optimizing ventricular activation sequence and APD distribution. *PLOS ONE* **17,** e0270559.

Nador F, Beria G, De Ferrari GM, Stramba-Badiale, M, Locati EH, Lotto A & Schwartz PJ (1991). Unsuspected echocardiographic abnormality in the long QT syndrome. Diagnostic, prognostic, and pathogenetic implications. *Circulation* **84**, 1530-42.

Napolitano C, Priori SG & Schwartz PJ (2000). Significance of QT dispersion in the long QT syndrome. *Prog Cardiovasc Dis* **42,** 345–350.

Nerbonne JM (2000). Molecular basis of functional voltage-gated K+ channel diversity in the mammalian myocardium. *J Physiol* **525,** 285–298.

Odening KE, Hyder O, Chaves L, Schofield L, Brunner M, Kirk M, Zehender M, Peng X & Koren G (2008). Pharmacogenomics of anesthetic drugs in transgenic LQT1 and LQT2 rabbits reveal

genotype-specific differential effects on cardiac repolarization. *Am J Physiol Heart Circ Physiol* **295,** H2264–H2272.

Odening KE, Jung BA, Lang CN, Cabrera Lozoya R, Ziupa D, Menza M, Relan J, Franke G, Perez Feliz S, Koren G, Zehender M, Bode C, Brunner M, Sermesant M & Föll D (2013). Spatial correlation of action potential duration and diastolic dysfunction in transgenic and drug-induced LQT2 rabbits. *Heart Rhythm* **10,** 1533–1541.

Odening KE & Koren G (2014). How do sex hormones modify arrhythmogenesis in long QT syndrome? Sex hormone effects on arrhythmogenic substrate and triggered activity. *Heart Rhythm* **11,** 2107–2115.

Odening KE, van der Linde HJ, Ackerman MJ, Volders PGA & ter Bekke RMA (2022). Electromechanical reciprocity and arrhythmogenesis in long-QT syndrome and beyond. *Eur Heart J* **43,** 3018–3028.

Pilia N, Nagel C, Lenis G, Becker S, Dössel O & Loewe A (2021). ECGdeli - An open source ECG delineation toolbox for MATLAB. *SoftwareX* **13,** 100639.

Quinn TA & Kohl P (2016). Rabbit models of cardiac mechano-electric and mechano-mechanical coupling. *Progress in Biophysics and Molecular Biology* **121,** 110–122.

Quinn TA & Kohl P (2021). Cardiac Mechano-Electric Coupling: Acute Effects of Mechanical Stimulation on Heart Rate and Rhythm. *Physiological Reviews* **101,** 37–92.

Roden DM (2004). Drug-Induced Prolongation of the QT Interval. *The New England Journal of Medicine*10.

Roden DM (2008). Long-QT Syndrome. *New England Journal of Medicine* **358,** 169–176.

Rudy Y (2017). Noninvasive ECG imaging (ECGI): Mapping the arrhythmic substrate of the human heart. *Int J Cardiol* **237**, 13-14.

Rudy Y & Burnes JE (1999). Noninvasive Electrocardiographic Imaging. *Annals of Noninvasive Electrocardiology* **4,** 340–359.

Sachs F (2009). Stretch-Activated Ion Channels: What Are They? *Physiology (Bethesda)* **1**, 50-6.

Schwartz PJ, MD LC & Insolia R (2012). Long QT Syndrome: From Genetics to Management. *Circ Arrhythm Electrophysiol* **5,** 868–877.

Solovyova O, Katsnelson LB, Kohl P, Panfilov AV, Tsaturyan AK & Tsyvian PB (2016). Mechano-electric heterogeneity of the myocardium as a paradigm of its function. *Prog Biophys Mol Biol* **120,** 249–254.

Taggart P, Sutton P, John R, Lab M & Swanton H (1992). Monophasic action potential recordings during acute changes in ventricular loading induced by the Valsalva manoeuvre. *Br Heart J* **67,** 221–229.

Opthof T, Meijborg VMF, Belterman CNW & Coronel R (2015). Synchronization of repolarization by mechano-electrical coupling in the porcine heart | Cardiovascular Research

Vijayakumar R, Silva JNA, Desouza KA, Abraham RL, Strom M, Sacher F, Van Hare GF, Haïssaguerre M, Roden DM & Rudy Y (2014). Electrophysiologic Substrate in Congenital Long QT Syndrome. Cardiovascular Research **108**, 181–187.

Winter J & Shattock MJ (2016). Geometrical considerations in cardiac electrophysiology and arrhythmogenesis. *EP Europace* **18,** 320–331.

Zaza A (2016). Electrophysiology meets geometry. *Europace* **18,** 317–317.

Ziupa D, Menza M, Koppermann S, Moss R, Beck J, Franke G, Perez Feliz S, Brunner M, Mayer S, Bugger H, Koren G, Zehender M, Jung BA, Seemann G, Foell D, Bode C & Odening KE (2019). Electro-mechanical (dys-)function in long QT syndrome type 1. *International Journal of Cardiology* **274,** 144–151.

Figure legends

Abstract Figure: Electromechanical reciprocity in healthy (control) and acquired long QT syndrome (aLQTS) rabbit hearts. **A.-B.** Electrical alteration in aLQTS. **A.** Exemplary ECG traces demonstrating I_{Kr}-blocker E-4031-induced RT prolongation in aLQTS. **B.** Visualization of heart rate corrected RTn370 (each color-coded scale includes 20ms) on rabbits' torso in aLQTS compared to control (n=6 each). **C.** Electro-mechanical coupling (EMC). Exemplary myocardial longitudinal velocity curve in base (cm/s) during cardiac cycle in control (blue) and aLQTS (red). Indicated are peak amplitudes (AMPsys, AMPdia) and time-to-diastolic peak (TTPdia). **D.** Mechano-electrical coupling (MEC). Box plots of preload induced changes in repolarization. Comparison between the timepoints *baseline* (15 sec before increase in preload) and time of the maximal RTn370 increase *peak-preload* (around 20 sec after NaCl bolus injection). Heart rate corrected RTn370 demonstrates more pronounced RT-changes in aLQTS compared to control (n=13 each).

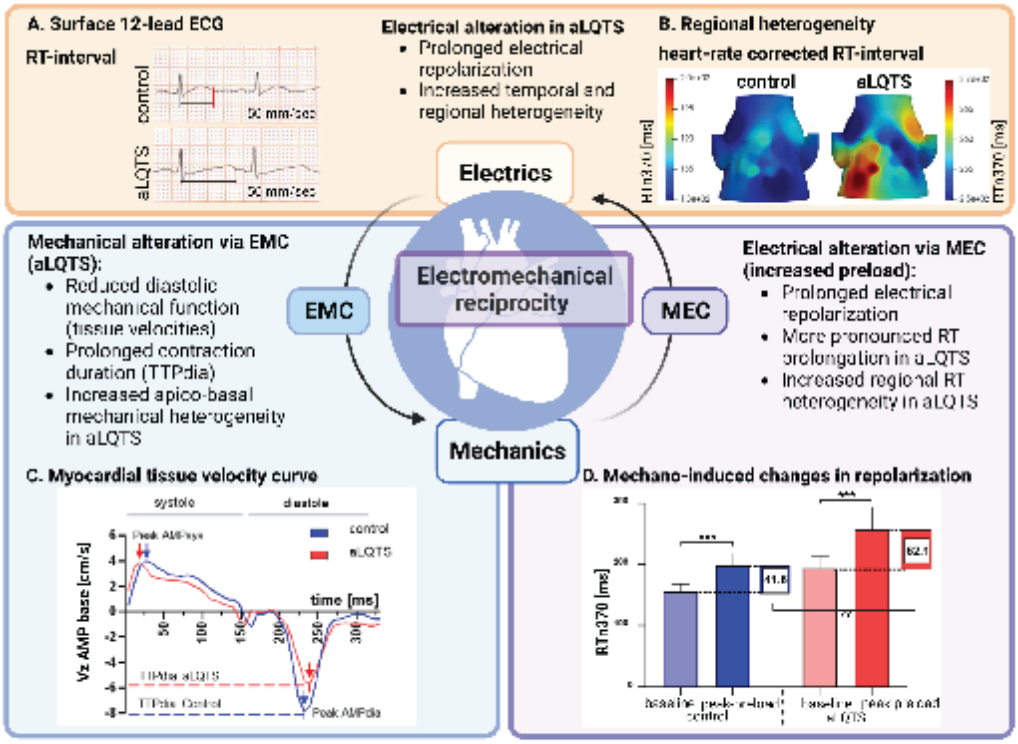

The Journal of Physiology

Figure 1: Optical mapping setup and examples of motion correction. **A.** Image of the panoramic optical mapping setup. Indicated are LEDs, mirrors, and the camera position. **B.** Illustration of the three different views of the heart (anterior, left-posterior, and right-lateral) and corresponding selected regions of interest (ROIs). **C.** Exemplary fluorescence tracings before and after motion correction. ∆F= change in fluorescence intensity in arbitrary units.

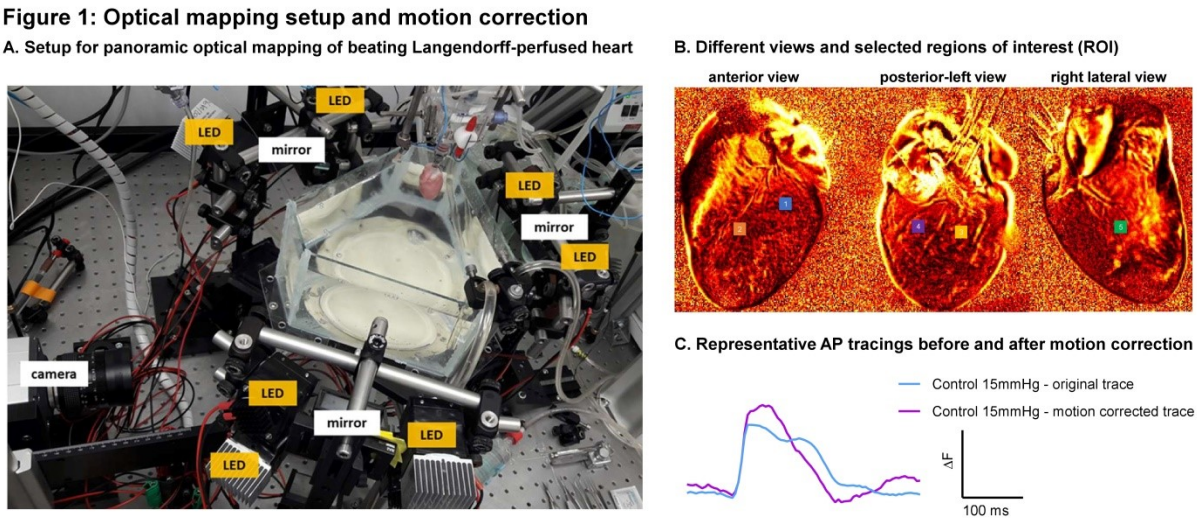

Figure 2: Electrical alterations in acquired LQTS (induced by I_{Kr}-blocker E-4031). **A.-D.** 12-lead surface ECG. **E.-J.** 24-lead ECG vest. **A.** Exemplary ECG traces demonstrating E-4031-induced RT prolongation in aLQTS. **B.** Dot plots graph indicating prolongation of RR-adjusted RTn370-interval in all individual rabbits after E-4031 administration compared to control (n=12 each). **C.** Dot plots graph indicating increased temporal RT-variability (short term variability of RT, STV_{RT}) in aLQTS compared to control (n=13 each). **D.** Dot plots graph demonstrating increased regional RT-dispersion (RT-dispersion (max-min)) in aLQTS compared to control (n=13). **E.** Dot plots graph demonstrating increased RV-LV dispersion (ms) in aLQTS compared to control (n=4). **F.** Schematic illustration of arrangement of ECG-leads on the ventral side of the 24-lead ECG vest (lead 5–24). **G.** CT-based modelling of the rabbits' torso and organs (left; dark-blue: bones, dark-green: cartilage, orange: heart, salmon: lungs, brown: liver; light-green: blood, yellow: stomach) and visualization of a transversal cut through the meshed geometry of the torso (right). **H.** Exemplary illustration of

automated ECG vest signal-annotation. **I.** Visualization of RTn370 (each color-coded scale includes 20ms) on rabbits' torso in aLQTS compared to control (n=6 each). **J.** Visualization of regional RT-heterogeneity (color-coded as differences compared to minimum RT) on rabbits' torso in aLQTS compared to control (n=6 each). E and F modified from (Moss *et al.*, 2022) with permission.

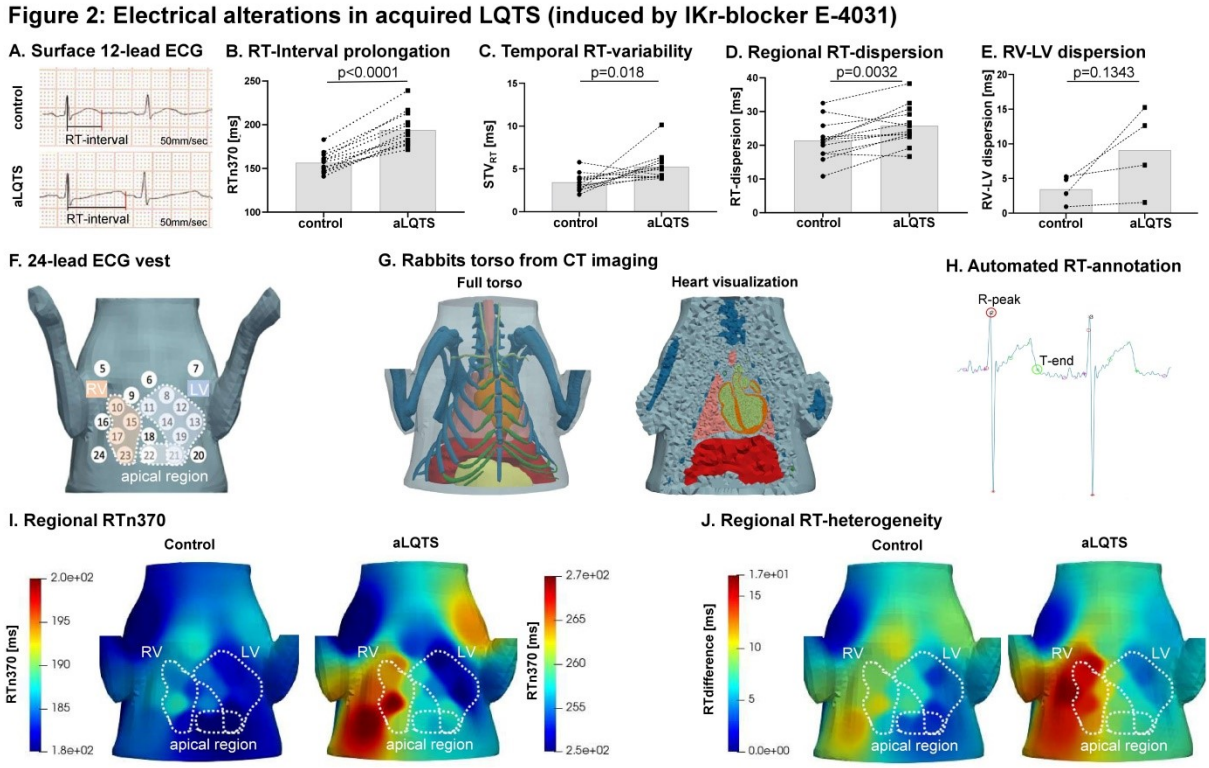

Figure 3: Impact of electrical alterations (aLQTS) on mechanical function (via EMC) in tissue-phase mapping MRI (TPM-MR). **A.** Example of regional longitudinal velocities (Vz AMP, cm/s, color-coded as indicated) and radial velocities (indicated by length of arrows) during cardiac cycle in control and aLQTS. **B.** Bull's eye plots of diastolic peak longitudinal velocities (Vz AMPdia, cm/s) in all basal, mid, and apical segments. Velocities are color-coded and average values are indicated. Diastolic peak longitudinal velocities decreased in 9 out of 16 segments as indicated in the arrow (n=19 each). **C.** Bull's eye plots of regional time-to diastolic peak duration in longitudinal velocities (Vz TTPdia, cm/s). Vz TTPdia increased in 9 out of 16 segments as indicated in the arrow (n=9 each). Velocities are color coded as indicated. **D.** Exemplary myocardial longitudinal velocity curve in base (Vz AMP

(cm/s)) during cardiac cycle in control and aLQTS. **E.** Box plot graph indicating decreased apico-basal heterogeneity in Vz AMPdia in aLQTS compared to control (n=19 each). **F.** Box plot graph indicating increased apico-basal heterogeneity in TTPdia in a LQTS compared to control (n=8 each). * p<0.05, ** p<0.01, *** p<0.001. Detailed mean and SD and exact p-values of the TPM-MRI measurements summarized in the bull's eye plots can be found up in the statistical summary document.

Figure 3: Impact of electrical alterations (aLQTS) on mechanical function (via EMC) in TPM-MR

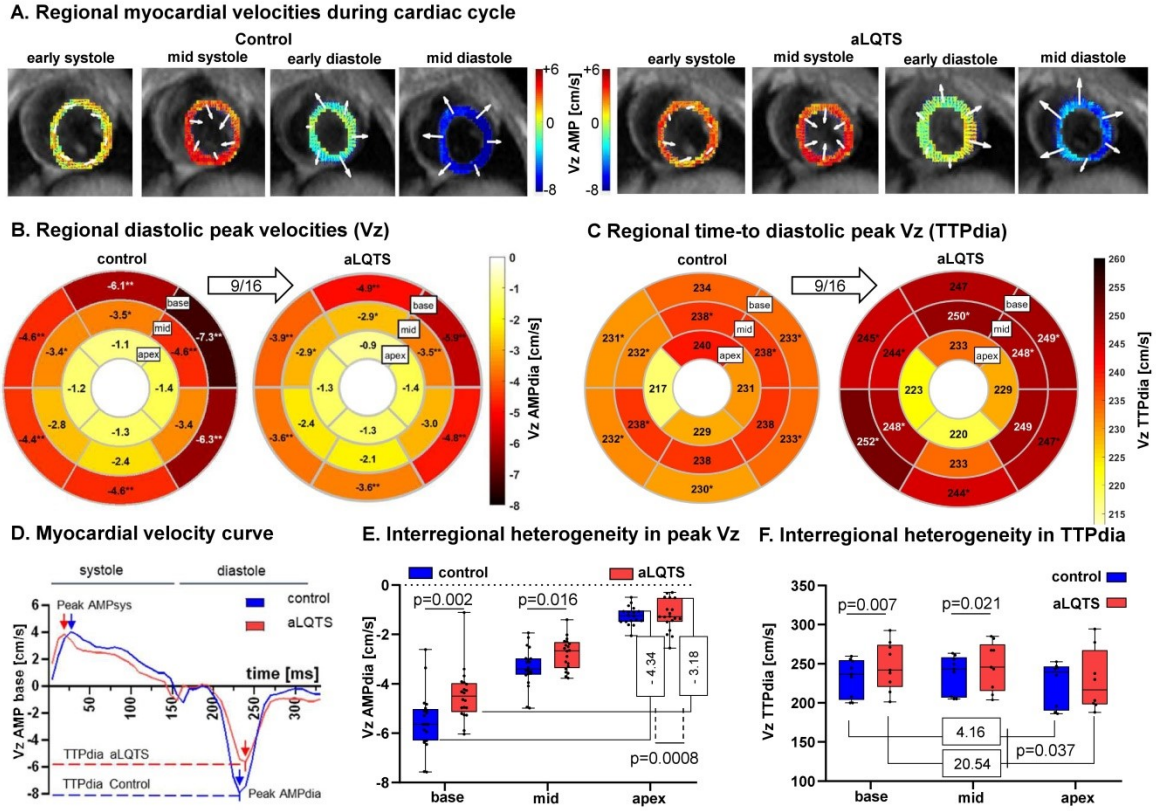

Figure 4: Impact of mechanical alteration (increase in preload) on electrical function (via MEC). **A.-B.** 12-lead surface ECG. **C.** 24-lead ECG vest. **A.** Mechanically induced changes in RR- and uncorrected RT-interval at baseline and NaCl-bolus-peak in both groups, control and aLQTS (n=13 each). **B.** Mechanically induced changes in cardiac repolarization. **B.1** Illustration of average RR-corrected RTn370-intervals over time (duration of bolus injection is indicated by "start" and "stop") demonstrates a mechano-induced RT-prolongation (n=13 each). **B.2** Box plots of baseline and peak heart rate corrected RTn370 demonstrates more pronounced RT-changes in aLQTS compared to control (n=13 each). **C.** Example of mechanically induced changes in temporal RT-heterogeneity (STV_{RT}) in control and aLQTS. (left panel: baseline; right panel: after NaCl-bolus; indicated are 15 beats before and 15 beats after peak RT) **D.** Visualization of mechanically induced changes in regional RT-heterogeneity (color-coded as differences compared to minimum RT) (n=6).

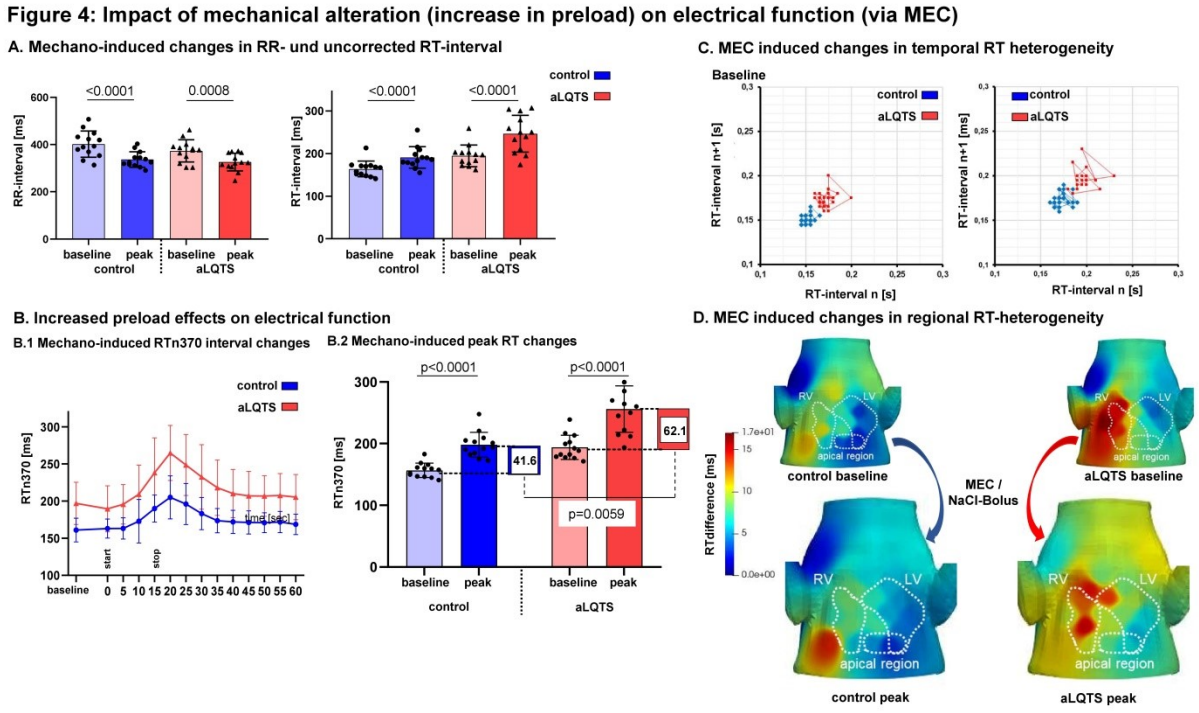

Figure 5: Mechano-induced changes in blood pressure and mechano-induced RT changes during autonomic blockade. **A.1** Comparison of mechano-induced changes in mean arterial blood pressure (MAP) [mmHg] (n=5 each). **A.2** Comparison of delta MAP (peak-baseline) between control and aLQTS (n=5 each). **B.** Mechano-induced RT changes during sympathetic and parasympathetic blockade. **B.1** Mechano-induced changes in RT before (control) and after (blockers) complete blockade of the sympathetic and parasympathetic system (n=8 each). **B.2** Comparison of mechano-induced RT changes (Delta-RT) demonstrates neither significant nor consistent differences in RT-changes between baseline and blocker experiments in the individual rabbits (n=8 each). **B.3** Comparison of heart rate before and after complete blockade of the sympathetic and parasympathetic system (n=8 each). **B.4** Illustration of average RR-corrected RTn370-intervals over time before and after complete blockade of the sympathetic and parasympathetic system (n=8 each).

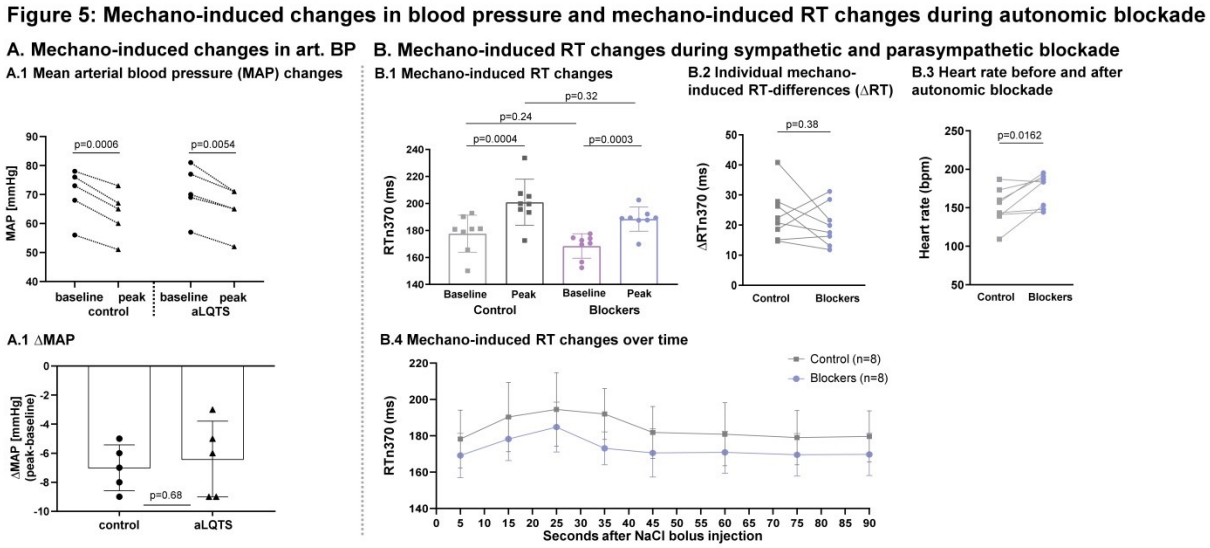

Figure 6: *Ex vivo* optical mapping assessment of MEC in Langendorff-perfused beating hearts. **A.** E-4031 induced changes in QT-intervals. **A.1** Original tracings of control and aLQTS ECGs during atrial stimulation (A-Stim). Indicated are QRS complex, T-wave and QT-intervals. **A.2** Bar graphs of E-4031 induced changes in QT. *** p<0.001, paired t-test. **B.** E-4031 induced changes in APD_{75} *ex vivo*. **B.1** Representative optical AP tracings in LV and RV at baseline (control) and after E-4031 perfusion (aLQTS) are shown. ΔF= change in fluorescence intensity in arbitrary units. **B.2** Bar graphs of APD_{75} in LV and RV ROIs in control and aLQTS in n=6 hearts (of note, for RV mid APD analyses only n=2 hearts could be used due to pronounced motion-artifacts in the other 4). * p<0.05, paired t-tests for each ROI. **B.3** Bar graphs of APD_{75} in LV and RV ROIs (B: base, M: mid, A: apex) in control and aLQTS visualizing regional heterogeneity. * p<0.05. **C.** Lack of MEC induced changes in QT-intervals and in APD_{75} *ex vivo* in n=6 hearts. **C.1** Bar graphs of QT at 6mmHg and 15mmHg in control and aLQTS. **C.2** Representative AP tracings in LV at 6mmHg and at 15mmHg preload in control and aLQTS are shown.